Progress In Electromagnetics Research B, Vol. 50, 113–140, 2013

ON THE FEASIBILITY OF 320 Gb/s ALL-OPTICAL AND GATE USING QUANTUM-DOT SEMICONDUCTOR OPTICAL AMPLIFIER-BASED MACH-ZEHNDER INTERFEROMETER

Evangelia Dimitriadou and Kyriakos E. Zoiros*

Lightwave Communications Research Group, Department of Electrical and Computer Engineering, School of Engineering, Democritus University of Thrace, 12 Vas. Sofias Str., Xanthi 67100, Greece

Abstract—The feasibility of realizing an all-optical AND gate for 320 Gb/s return-to-zero data by incorporating quantum-dot semiconductor optical amplifiers (QD-SOAs) in a Mach-Zehnder interferometer (MZI) is theoretically investigated and demonstrated. The proposed scheme employs the QD-SOA-based MZI in a configuration where the QD-SOA in one MZI arm is subject to the first data sequence, the QD-SOA in the other MZI arm receives no such input but is constantly held in the small signal gain regime, and the second data stream is inserted from the common MZI port acting as enabling or disabling signal. Compared to other approaches adopted for the same purpose this implementation is more general, direct, flexible and affordable as only one strong data signal is required to control switching. By conducting numerical simulation the impact of the critical parameters on the Q-factor is thoroughly assessed. The obtained results are interpreted with the help of a complete characterization of the QD-SOA response to an ultrafast data pulse stream. This allows to specify the requirements that the critical parameters must satisfy to achieve acceptable performance. The extracted design rules are technologically realistic and ensure AND operation both with logical correctness and high quality. The outcome of the numerical treatment extends the range of Boolean functions executed with the QD-SOA-MZI module at sub-Tb/s data rates.

Received 31 January 2013, Accepted 28 March 2013, Scheduled 2 April 2013

* Corresponding author: Kyriakos E. Zoiros (kzoiros@ee.duth.gr).

1. INTRODUCTION

All-optical gates constitute key building units for the development of lightwave broadband communications networks through the execution of signal processing functionalities without problematic optoelectronic conversions at the photonic nodes [1]. In particular the AND gate is indispensable for achieving this goal as it is involved in the accomplishment of numerous tasks in the optical domain both in fundamental and system-oriented level, such as buffering [2], address comparison [3], add-drop multiplexing [4], packet clock and data recovery [5], packet header and payload separation [6], binary pattern recognition [7], binary counting [8], analog-to-digital conversion [9], digital encoding and comparison [10], data regeneration [11], waveform sampling [12], half addition [13], multiplication [14], construction of other logic gates [15] and of combinational logic circuits [16]. Given its important, multi-lateral role the AND gate has attracted intense research interest and among the technological options that exist for its implementation those that exploit a semiconductor optical amplifier (SOA) are well established [17]. In fact, besides being employed for classical applications such as signal generation [18], amplification [19] and modulation [20], SOAs have also demonstrated their potential as nonlinear switching elements for performing all-optical AND logic, either as stand-alone entities [21–27] or incorporated in an interferometric configuration [28–32].

Nevertheless, the extension of the use of these digital logic modules as AND gate at ultrafast data rates is limited by the inherently slow SOA gain recovery time and the associated pattern-dependent performance degradation [33]. The negative by-product of this fact is that it is not possible to satisfy the unceasing demand for more bandwidth since single channel data rates are upgrading to magnitudes that exceed by far the SOAs ultrafast potential [34]. Although methods such as injection of a continuous wave (CW) strong holding beam [35], external filtering [36, 37], special switch architectures [38] and differential schemes [39, 40] have been proposed to address this issue, they lack design flexibility, switching power efficiency, cost effectiveness, easiness of setup adjustment, 'on-the-fly' processing capability and simplicity of logical outcome formation. Also they suffer from noise accumulation, signal-to-noise reduction, useful information elimination, input signal difficult precise synchronization and phase shift discrepancy from desired switching level. Therefore these solutions present practical and technical constrains, which enable them to support only a very small fraction of the excessively increasing line rates that are currently underway [34] and soon or later will be

running in future optical networks.

In order to keep properly pace with this trend a different and novel technological path should be followed, which should have the perspective of responding to this modern challenge in a more general, direct, flexible and affordable manner. In this context quantum-dot (QD) SOAs with their special structure are very promising devices thanks to their distinctive physical properties that have been constantly improving during recent years over conventional SOAs. These include the lower threshold current, the higher saturation output power, the wider gain bandwidth, the lower noise figure, the low polarization gain dependence, the weaker temperature sensitivity and their exceptional faster gain recovery time [41–44]. The latter characteristic allows them to respond much quicker to ultrafast data compared to SOAs that don't have QDs inserted in their active region and thus they can achieve pattern-free operation more easily. These combined advantages have made QD-SOAs ideal candidates for all-optical signal processing [45, 46]. In parallel the Mach-Zehnder interferometer (MZI) is most suitable for this purpose as it effectively combines the structural simplicity, the co-propagation of the launched signals and the low switching energy requirement with the potential for integration and the overall practicality [47].

Owing to its attractive features the QD-SOA-based MZI has been the primary choice for the demonstration of all-optical logic functions [48–56]. In fact it has been theoretically predicted that it should be capable of Boolean AND operation up to a quarter of Tb/s [48]. However the way proposed for realizing this gate in [48] raises some important issues, which leave enough margins for further research and improvement towards the achievement of ultrafast operation. More specifically, the concept of the scheme relies on driving the SOA in the upper MZI arm with one of the data signals that participate in the AND operation, and the SOA in the lower MZI arm with a temporally shifted version of the same signal. This relative delay between the original signal and its replica changes the phase of the other involved data signal, which is switched at the output. Thus this parameter is critical for the performance of the scheme and the ability to operate at ultrafast data rates is inversely proportional to it. In other words, the faster the desired data rate the smaller this delay should be, which as we move closer to the sub-Tb/s scale may be hard to achieve with the appropriate degree of accuracy and synchronization. Furthermore, the need for this delay limits the possibility of performing real time signal processing, i.e., 'on-the-fly', at photonic nodes by means of the AND gate and the applications that it supports. This happens because as data pulses arrive more often it

becomes quite difficult to set the temporal offset that the incoming stream of information must undergo. Similarly the existence of the specific delay may cause an additional latency in combinatorial and sequential all-optical circuits and subsystems where the AND gate is the basic building block. Finally, the launch of a delayed copy of the data signal into the second SOA imposes a greater, unnecessary strain on the gain dynamics of this device and hence on the overall operation of the scheme, at the expense of making it more power consuming and complex to adjust and optimize.

The above reasoning designates that the extension of the AND gate's ultrafast capability dictates to use a different configuration of the QD-SOA-based MZI. For this purpose we propose in this paper a more simple, affordable and versatile way of tackling the specific task by using the classic MZI scheme [31]. The adopted approach requires only two distinct data trains between which the AND function is directly executed, with only one of them being strong and inserted in only one QD-SOA, thus eliminating the need for delaying the same data stream and helping avoid the associated drawbacks. The feasibility of the scheme is thoroughly investigated by applying a numerical model that takes into account the dynamical behaviour of QD-SOAs in order to simulate the operation of the standard MZI configured as AND gate when it receives a pair of fully-loaded pseudorandom binary sequences (PRBS) as inputs. This is done at 320 Gb/s, where so far efforts with the QD-SOA-based MZI in single rail switching mode have included only demultiplexing [57]. However in this application many data pulses travel intact through the interferometer without being transmitted at the output. In contrast in this paper we are interested in the more general and demanding situation where every bit of information is involved in the process of switching. This fact imposes a greater strain on the QD-SOA gain dynamics and accordingly makes the selection of the critical parameters more tight [58]. Nevertheless it will be shown that the conducted theoretical analysis allows to thoroughly investigate and assess the impact of these parameters on the metric of Q-factor. Then we extract a set of design rules for their selection and combination within their specified allowable range so that the AND function can be executed at the target ultrafast data rate both with logical correctness and high quality. The presented work extends and complements our previous research on all-optical gates using as switching module the QD-SOA-based MZI [52–56]. Its outcome can contribute to the practical implementation of the AND gate and of the diverse applications it is destined to serve as core logical unit at ultrafast line rates. In this manner the tremendous capacity offered by fibre will be exploited to an enhanced degree towards the better

satisfaction of modern telecommunications networks' various demands.

2. QD-SOA STRUCTURE

The schematic diagram of a QD-SOA is shown in Fig. 1(a). This device is equivalent to a conventional SOA in terms of its basic structure and applications but its active region consists of multiple QD layers [33, 59]. The fabrication of these QDs is based on a self-assembled growth technique called Stranski-Krastanov. Initially this involves the growth of a two-dimensional layer, namely the wetting layer. When a critical layer thickness is exceeded, then three-dimensional islands are formed on top of the wetting layer [60, 61]. QD-SOAs operating in the 1550-nm range consist of InAs QDs grown on InP substrate [44, 62]. Assuming that the conduction band of a single QD has two discrete electronic states, namely the ground state (GS) and the exited state (ES), and that the wetting layer offers an additional energy level (WL), a QD-SOA is considered to be a three level system. Owing to the discrete nature of the energy band diagram of the QDs, QD-SOAs acquire special dynamic characteristics and exhibit remarkable optical properties. Fig. 1(b) depicts the energy band diagram of a QD system and the WL as well as the basic electron transitions among the three energy states of the conduction band. Electrons are assumed to limit the carrier dynamics, since holes have larger effective mass resulting in smaller level spacing and thus faster relaxation [41, 63]. The carrier capture directly into the GS is also not taken into account due to fast intradot carrier relaxation and large energy separation between the

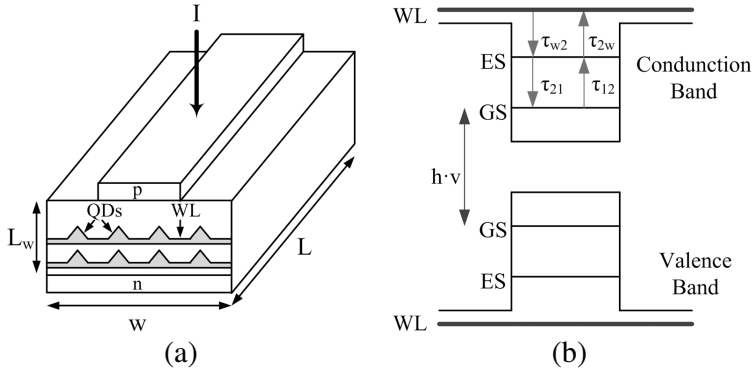

Figure 1. (a) Schematic diagram of a QD-SOA, (b) energy band diagram of a QD system and the WL.

GS and the WL band edge [41]. Furthermore, the holes are assumed to be in quasi thermal equilibrium at all times [41, 63]. Therefore the full set of transitions includes [50] (a) the electron transitions between the WL and the ES, which are characterized by the transition times τ_{w2} and τ_{2w}, (b) the electron transitions between the ES and the GS, which are characterized by the transition times τ_{21} and τ_{12}, and (c) the spontaneous recombination in the WL and the QDs. In particular carriers are injected in the WL through electrical pumping and due to phonon- and Auger-assisted processes [33, 41] they relax to the ES. Similarly carriers from the ES relax to the GS, while the amplification process is incited by the stimulated radiative transition from the GS of the conduction band to the GS of the valence band. In this manner the states above the GS serve as a carrier reservoir for the GS [33, 62, 63], which accelerates the QD-SOA gain recovery and accordingly its response to ultrafast excitations.

3. PRINCIPLE OF OPERATION OF PROPOSED AND GATE

The configuration of the proposed AND gate considered in the conducted theoretical treatment is shown in Fig. 2. It is based on the symmetrical MZI architecture, in which the same QD-SOAs, QD-SOA1 and QD-SOA2, are placed in the upper and lower arm, respectively. A data-carrying signal A enters through a wavelength selective coupler (WSC) QD-SOA1, while a data-carrying signal B is inserted in the MZI and is split via the input 3 dB coupler C1 into a pair of identical parts, which travel separated along the QD-SOAs located in their path. Signal A should be at least an order of magnitude stronger than signal B [49]. These signals are discriminated by using different wavelengths, such that their detuning in the 1550 nm region is less than

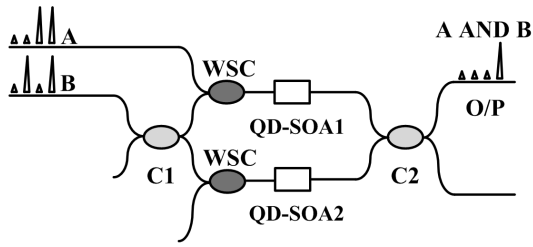

Figure 2. Simulated setup of QD-SOA-based MZI configured for Boolean AND operation between data A and B produced at output port (O/P). C1 and C2: 3 dB couplers. WSC: wavelength selective coupler. QD-SOA: quantum-dot semiconductor optical amplifier.

the homogeneous broadening of QD-SOA1 [49, 51]. In this manner only signal A can modify the nonlinear optical properties of QD-SOA1 and induce a change on the gain and phase of signal B. Now if B = '0' then regardless of the binary content of A we get nothing at output port (O/P), simply because there is no input signal on which to imprint any perturbation of the initially balanced MZI and to transfer to the O/P. This is a trivial situation, which changes when B = '1', namely when data sequence B contains a pulse. In this case the result at O/P depends on the existence or not of a pulse in the same bit slot of data sequence A. More specifically, if A = '0', QD-SOA1 remains intact to the same dynamical state as QD-SOA2 so that the decomposed constituents of B perceive the same gain. Thus when they recombine at 3 dB coupler C2 they interfere destructively, which results in a space at O/P. But if A = '1' QD-SOA1 undergoes a radical change of its gain compared to the non-driven QD-SOA2. Consequently the copy of B in the upper MZI arm acquires via cross-phase modulation [64] a nonlinear phase shift against its counterpart in the lower MZI arm, which eventually creates a relative phase difference between these components. If this quantity is ideally made equal to π then it is possible to maximize the amount of the power that emerges at O/P and hence the amplitude of the obtained mark. According to this mode of operation a pulse occurs at O/P if and only if a pulse is present in both signals A and B whilst no pulse appears at the specific terminal if a pulse is absent from either A or B or from both of them. In other words O/P = '0' when A, B = '0, 0', '0, 1' or '1, 0', and O/P = '1' when A, B = '1, 1'. These combinations of logical pairs and their outcome form the truth table of Boolean AND logic executed between A and B, which means that the QD-SOA-based MZI in the setup of Fig. 2 is configured as AND gate.

4. MODELING

In this section we formulate the model that is used to study and assess the performance of the AND gate implemented with the QD-SOA-based MZI. According to the principle of operation of this gate the model comprises of two parts. In the first part the equations that concern propagation of a strong optical pulse along a QD-SOA are presented and the approach followed to numerically solve them is described. In the second part, starting from the expression of the power that emerges from a MZI with nonlinear active elements placed in its two arms, it is explained how the AND gate can be simulated with the aid of the relevant information provided for the QD-SOAs in the first part.

4.1. Stand-alone QD-SOA

The model that is employed to describe the operation of the stand-alone QD-SOA takes into account the propagation of a strong optical pulse along the longitudinal direction, z, of the QD-SOA in conjunction with the change of its gain dynamics. For this purpose we treat the QD-SOA as a three-level system according to the energy band diagram described in Section 2. This approach allows us to obtain realistic, accurate and global results, like in research efforts of nature similar to ours [49, 51]. It also complies with the relevant finding that the major contribution to the ultrafast gain recovery of QD-SOAs is made by the cascade of the dynamical process, which includes indirect relaxation, from the WL via the ES into the GS [65]. In comparison, if it is assumed that the QDs' conduction band, and accordingly its valence band, consists of the GS only, then although the influence of the direct relaxation channel can be explicitly taken into account, the carrier kinetics cannot account quantitatively for the exceptionally fast QD-SOA gain recovery [65]. However it is exactly owing to this unique property that QD-SOAs can be exploited as nonlinear elements for executing all-optical logic functions at sub-Tb/s data rates. Moreover, the absence of the intermediate ES state is replaced by calculating the carrier occupation probability near the band edge of the WL, which in turn is populated by the injection current and serves as a reservoir of carriers. As a consequence this modeling approach is valid when the population of carriers in the WL is large [66]. Hence it is restricted to specific QD-SOAs driving conditions and leads to overestimated predictions for the capability of QD-SOAs to be incorporated in interferometric configurations for all-optical logic purposes, such as the Boolean AND operation [48]. Therefore the 3-level rate equation model (3LREM) we have adopted for the QD-SOAs dynamical behavior is mostly suitable for simulating the operation and assessing the feasibility of the QD-SOA-based MZI AND gate at 320 Gb/s.

Following [67], the model is formulated by the propagation Equation (1) and the 3-level rate Equations (2)–(4) for the wetting layer (WL), excited state (ES) and ground state (GS), respectively

$$\frac{\partial S}{\partial z} = \left[g_{\max}\left(2f-1\right) - \alpha_{\text{int}}\right] S \tag{1}$$

$$\frac{\partial N_w}{\partial t} = \frac{J}{eL_w} - \frac{N_w(1-h)}{\tau_{w2}} + \frac{N_Q h}{L_w \tau_{2w}} - \frac{N_w}{\tau_{wR}} \tag{2}$$

$$\frac{\partial h}{\partial t} = \frac{L_w N_w (1-h)}{N_Q \tau_{w2}} - \frac{h}{\tau_{2w}} - \frac{(1-f)\,h}{\tau_{21}} + \frac{f\,(1-h)}{\tau_{12}} \tag{3}$$

$$\frac{\partial f}{\partial t} = \frac{(1-f)\,h}{\tau_{21}} - \frac{f(1-h)}{\tau_{12}} - \frac{f^2}{\tau_{1R}} - \frac{g_{\max}\,(2f-1)\,L_w V_g}{N_Q} S \tag{4}$$

These equations hold for a negligible QD-SOA facet reflectivity and amplified spontaneous emission (ASE) [49, 51], which as explained and justified in detail in [56] are valid assumptions that greatly simplify the model's formulation. Furthermore, the homogeneous broadening is physically taken into account through the detuning of data-carrying signals A and B, whose angular frequencies must satisfy the condition $|\omega_A - \omega_B| \ll \gamma_{\text{hom}}$, where γ_{hom} is the homogeneous linewidth, in order to enable ultrafast single rail switching [64]. A special consideration of this effect would be necessary if the pursued goal were to perform some multi-wavelength task [68], where different input channels that are located within the homogeneous broadening interact strongly via cross-gain modulation (XGM). This nonlinear effect can also manifest if the detuning between signals A and B is sufficiently large compared to the inhomogeneous broadening, which occurs due to fluctuations in QD size and material composition [45]. In this case the QD ensemble should be divided into different groups with energies depending on their resonant frequencies. Then the QD-SOA dynamical behavior should be described by properly modifying the system of 3-level rate equations [63] while discriminating the modal gains of signals A and B by assuming a Gaussian-like distribution for their spectral profiles [62]. Nevertheless, although this possibility of XGM in QD-SOAs would be beneficial for multi-wavelength applications [45], yet the switching scheme we have proposed aims at realizing ultrafast Boolean logic operation on single channel data rates and hence at supporting all-optical signal processing in the context of Optical Time Division Multiplexing (OTDM) [69].

In relationships (1)–(4), variable t is time transformed into a retarded frame moving with the pulse [50] and the functions involved in the derivatives are the photon density of the driving data signal, $S = S(z,t) = P(z,t)/(A_{\text{eff}} V_g h\nu)$ (where $A_{\text{eff}} = 0.75\,\mu\text{m}^2$ is the effective cross section of the QD-SOA, $V_g \approx 8.3 \times 10^7$ m/s is the group velocity of the propagating signal and $h\nu$ the photon energy), the electron density in the WL, N_w, and the electron occupation probabilities in the ES and GS, h and f, respectively. Also $g_{\max} = l \frac{2N_Q}{L_w} \sqrt{\pi \ln 2} \frac{\gamma_{\text{hom}}}{\gamma_{\text{inhom}}} \sigma_{\text{res}}$ is the maximum modal gain, where l, N_Q and L_w is the number, surface density and effective thickness of the active QD layers, γ_{hom} is the homogeneous linewidth of the resonant QDs, γ_{inhom} the inhomogeneous linewidth of the QD ensemble and σ_{res} is the resonant cross section of

the carrier-photon interaction [70]. Furthermore, α_{int} is the material absorption coefficient, J the injection current density, e the electron charge, τ_{w2} the electron relaxation time from the WL to the ES, τ_{2w} the electron escape time from the ES to the WL, τ_{wR} the spontaneous radiative lifetime in the WL, τ_{21} the electron relaxation time from the ES to the GS, τ_{12} the electron escape time from the GS to the ES and τ_{1R} the spontaneous radiative lifetime in the QDs.

The system of coupled Equations (1)–(4) is numerically solved in a step-wise manner for pulses that belong to a data signal. For this purpose, each input pulse is sampled over its period at discrete intervals, Δt, while the QD-SOA is divided into n uniform segments of length Δz, as shown if Fig. 3. The 4th order Runge-Kutta method is then applied on the created spatio-temporal grid of size $\Delta t \times \Delta z = 0.05\,\text{ps} \cdot \mu\text{m}$ to find the amplification factor, which by definition is $G(t) = S(L,t)/S(0,t)$, where $L = 4\,\text{mm}$ is the QD-SOA length. This procedure is followed for typical QD-SOA parameters' values taken from the literature [49–51, 70], which include $\alpha_{\text{int}} = 2\,\text{cm}^{-1}$, $L_w = 0.25\,\mu\text{m}$, $N_Q = 5 \times 10^{10}\,\text{cm}^{-2}$, $\sigma_{\text{res}} = 1.06 \times 10^{-19}\,\text{m}^2$, $\tau_{w2} = 3\,\text{ps}$, $\tau_{2w} = 1\,\text{ns}$, $\tau_{wR} = 0.2\,\text{ns}$, $\tau_{1R} = 0.4\,\text{ns}$ and $\tau_{12} = 1.2\,\text{ps}$.

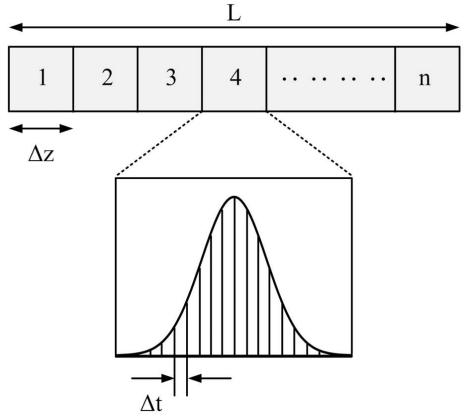

Figure 3. The considered spatio-temporal grid on which the 4th order Runge-Kutta method is applied. L: the QD-SOAs length. n: the number of uniform segments that the QD-SOA is divided into. Δz: the length of each spatial segment. Δt: the temporal interval between two consecutive samples of an input pulse.

4.2. MZI with QD-SOA

The simulation of the QD-SOA-based MZI when configured as AND gate according to Fig. 2 requires theoretically expressing the amount of power that is transferred to O/P as a result of A AND B operation. This is given by [49–51]

$$P_{O/P}(t) = \frac{1}{4}\left\{G_1(t)+G_2(t)-2\sqrt{G_1(t)G_2(t)}\cos\left[-\frac{\alpha_{\text{LEF}}}{2}\ln\left(\frac{G_1(t)}{G_2(t)}\right)\right]\right\}P_B(t) \quad (5)$$

where $G_1(t)$ and $G_2(t)$ are the time-dependent gains experienced by the constituents of data signal B in QD-SOA 1 and 2, respectively. $P_B(t)$ is the power of data signal B and α_{LEF} the linewidth enhancement factor of the QD-SOAs. From Equation (5) it is apparent that in order to calculate the power emerging from O/P it is necessary to know gains $G_1(t)$ and $G_2(t)$. For $G_1(t)$ this is done by solving numerically the system of Equations (1)–(4) for QD-SOA1 and input data signal A. The pulses of this signal belong to a 320 Gb/s return-to-zero (RZ) pseudo-random binary sequence (PRBS) of word length 2^7-1. Furthermore, their power profile is Gaussian, i.e., $P_A(0,t) = P_{\text{peak}}\exp[-4\ln 2(t/T_{\text{FWHM}})^2]$, where P_{peak} is their peak power and T_{FWHM} is their full-width at half-maximum, which corresponds to 35% of the operating period. Also in order to conduct a simulation analysis as realistic as possible the spaces of data signal A are not fully extinguished. This means that the extinction ratio (ER) of this signal, which is defined as the ratio of the minimum peak power of the marks to the maximum peak power of the spaces, is finite and specifically 10 dB. On the other hand things are simpler for QD-SOA2 since no strong data signal is inserted in it and consequently its gain dynamics are not altered. This means that the specific device will be constantly operating in the linear gain regime. Hence, by integrating both sides of (1) over the QD-SOA length and noting that under this operating condition the electron occupation probability in the GS remains unity, we obtain $G_2(t) = \exp[(g_{\max}-\alpha_{\text{int}})L] = G_{ss}$, where G_{ss} is the small signal gain being the same for both QD-SOAs. Finally $G_1(t)$ and $G_2(t)$ are replaced in (5) to find the light intensity at O/P for a data signal B having the same shape and temporal characteristics as A, perfect ER, and power content as mentioned in Section 3. This is done for $\alpha_{\text{LEF}} = 5$, which lies in the range of values for practical QD-SOAs with gain in the 1550 nm region [71].

5. QD-SOA CHARACTERIZATION

Given the central role of the QD-SOA in the operation of the MZI configured as AND gate it is important to characterize the dynamical behaviour of this device with respect to several critical operational parameters. This is necessary in order to be able to properly interpret in Section 6 the simulation results obtained when QD-SOAs are incorporated in the MZI. This task has not been addressed before in the way done in this paper. In fact the information given by other reported works [49–51, 57, 72] as part of the study on the performance of a QD-SOA-based MZI intended for use in the implementation of all-optical logic gates at ultrafast bit rates is not sufficient or complete for the pursued goal. More specifically, [50, 51] have dealt with the QD-SOA carrier dynamics and the temporal evolution of the occupation probabilities in the discrete levels of the QD system. In [72] the temporal dependence of the gain has been obtained both for a single input pulse and a non return-to-zero (NRZ) input pulse train. In the first case the result concerns the saturation and quick recovery of the QD-SOA caused by the pulse as it enters and leaves the device, respectively. In the other case the focus is on the gain that is modulated by the NRZ input pulse train and it is shown to respond directly to the input data pattern, i.e., the gain is saturated as long as logic ones enter the QD-SOA and it recovers when one or more logic zeros appear at the input. The same study examines also the change of the QD-SOA gain dynamics by a NRZ input pulse train for different values of τ_{21}, which shows that the decrease of this parameter speeds up the gain recovery of the QD-SOA. Moreover in [49], the temporal dependence of the gain is derived for the case of a single input RZ pulse and for different values of J and τ_{w2}. The results for J indicate that the increase of this parameter accelerates the gain recovery of the QD-SOA, while the results for τ_{w2} reveal that this parameter is a limiting factor for the QD-SOA gain dynamics. Finally, regarding the QD-SOA saturation properties, in [72] the steady-state static gain has been obtained as a function of the input power for different values of J, which shows that the gain begins to saturate as the input power is increased and that the saturation power is increased with J. This dependence on J can also be noticed in [57], where the 3 dB input saturation power, $P_{\mathrm{in,sat}}$, is calculated as a function of J for different values of QD-SOA length. This unveils that if the current density is kept constant the QD-SOA saturation power is decreased as its length is increased. This means that the longer the device is, the more easily it can be saturated by a smaller input power.

Despite the significant contribution of the aforementioned works,

a more comprehensive characterization of a QD-SOA intended for use as nonlinear element for interferometric switching should take into account the impact of a whole set of critical parameters. This task is of a greater importance when the mode of operation is pulsed and the strain imposed on the operating conditions is quite demanding [46], as in our case. Therefore we have focused on the QD-SOA gain dynamics and their dependence on these parameters, since it is expected that they will affect the performance of the proposed AND gate. More specifically, in Figs. 4 and 5 we examine the instantaneous QD-SOA gain variation for different values of the critical parameters, P_{peak}, G_{ss}, J, and τ_{21}. This task is accomplished for a single pulse only, which has been selected to be the last mark in the longest run of these bits inside the PRBS. This is done in order to ensure that a saturation equilibrium has been established for the QD-SOA gain dynamics and thus that the conducted characterization is as realistic as possible. For this purpose the process that is followed is to change each time one parameter while keeping the rest constant. More specifically the typical values chosen to be fixed for G_{ss}, J and τ_{21} are 15 dB, 0.8 kA/cm^2 and 1.5 ps, respectively. On the other hand the choice for the peak input data power has been dictated by the gain saturation of the QD-SOA that occurs under pulsed mode of operation. In this context the saturated gain, which is defined as the minimum of the instantaneous

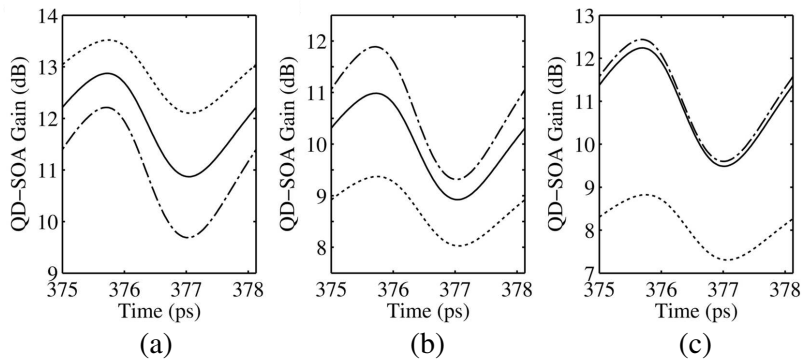

Figure 4. Instantaneous QD-SOA gain variation for (a) $P_{\text{peak}} = 4.5$ dBm (dotted line), $P_{\text{peak}} = 7$ dBm (solid line) and $P_{\text{peak}} = 9$ dBm (dash-dotted line), (b) $G_{ss} = 10.8$ dB (dotted line), $G_{ss} = 13.2$ dB (solid line) and $G_{ss} = 14.8$ dB (dash-dotted line), (c) $J = 0.3\,kA/cm^2$ (dotted line), $J = 1$ kA/cm^2 (solid line) and $J = 1.5$ kA/cm^2 (dash-dotted line).

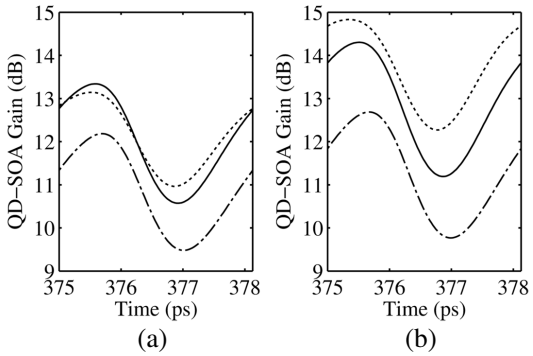

Figure 5. Instantaneous QD-SOA gain variation for $\tau_{21} = 0.3\,\text{ps}$ (dotted line), $\tau_{21} = 0.6\,\text{ps}$ (solid line) and $\tau_{21} = 1.4\,\text{ps}$ (dash-dotted line). (a) $J = 0.8\,\text{kA/cm}^2$, (b) $J = 2\,\text{kA/cm}^2$.

gain that is dropped after the pulse has acted on the QD-SOA, has been plotted as a function of this parameter in Fig. 6. From this figure we see that the 3 dB saturation input power [41] is $P_{\text{in,sat}} = 5\,\text{dBm}$. Thus in order for the QD-SOA to be adequately saturated for the needs of this characterization while at the same time keep P_{peak} reasonable we set $P_{\text{peak,fixed}} = 9.5\,\text{dBm}$. The incremental deviation of this fixed value from the 3 dB QD-SOA saturation input power under pulsed mode of operation defines an interval, which is indicated in Fig. 6 by the vertical dotted lines and the arrows attached on either side of them. The extent of this interval is determined by the, dimensionless, relative difference $\Delta P = P_{\text{peak,fixed}} - P_{\text{in,sat}} = 4.5\,\text{dB}$, within which the QD-SOA single-pass gain has been reduced by 5.5 dB. Therefore the remarks that will be extracted for the QD-SOA characterization conducted under the specific bias condition will also hold for a lower saturation level.

Figure 4(a) shows the instantaneous QD-SOA gain variation for different values of the peak input data power. First, it is observed that the initial level of the gain is not its small signal value, which also holds for Figs. 4(b)–(c) and 5(a)–(b). This happens because as already mentioned the examined pulse is the last of successive marks. For this reason when this pulse enters the QD-SOA it encounters a gain that has been partially recovered after it has been saturated by the preceding mark. Now the amount that the gain is dropped from its small signal value, ΔG, becomes larger as P_{peak} is increased. This is consistent with Fig. 6 and the fact that as P_{peak} is changed in this direction the QD-SOA becomes more saturated because of carrier depletion. Furthermore, this gain drop is favourable to impart a

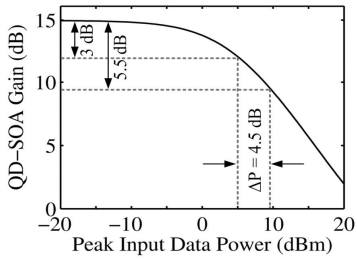

Figure 6. Variation of minimum instantaneous QD-SOA gain versus peak input data power. The difference $\Delta P = 4.5\,\text{dB}$ denotes the deviation of the QD-SOA bias point chosen as fixed for the simulation analysis from the 3 dB input saturation power.

differential phase between the decomposed components of data signal B as close as possible to π and hence achieve full switching. Then the dynamic gain response for different values of the QD-SOA small signal gain is illustrated in Fig. 4(b). Notably the drop of the gain from its unsaturated value is greater for larger small signal gain. More specifically, for $G_{ss} = 10.8\,\text{dB}$ the drop is $\Delta G \approx 2.8\,\text{dB}$, while for $G_{ss} = 14.8\,\text{dB}$ $\Delta G \approx 5.5\,\text{dB}$. Thus similarly to the case of the peak input data power the extent of the QD-SOA saturation quantified by ΔG becomes larger as G_{ss} is increased, which as mentioned is helpful for creating the desired phase difference between the MZI arms. Moreover, Fig. 4(c) shows the instantaneous QD-SOA gain variation for different values of current density. The increase of J from 0.3 to $1\,\text{kA/cm}^2$ supplies the GS with more carriers that are available for the gain recovery process and thus the latter is accelerated. However, if J is further increased to $1.5\,\text{kA/cm}^2$ the effect on the dynamical behavior of the gain is not so pronounced. This happens because the ES and WL, which act as carrier reservoirs for the GS, have been adequately filled and the additionally supplied carriers do not fully participate in the QD-SOA gain recovery process. Finally, in Fig. 5(a) we present the instantaneous QD-SOA gain variation for different electron relaxation times from the ES to the GS and for the chosen fixed value of current density. With the decrease of τ_{21} from 1.4 to 0.6 ps carriers relax faster from the ES to the GS and so the process of gain recovery is made faster. At the same time there are more carriers involved in the amplification process which leads to less intense saturation and gain modulation. This also holds for the case in which τ_{21} is decreased down to 0.3 ps. But when the QD-SOA becomes saturated subject to the consecutive bits of the PRBS, more carriers relax to the GS. Therefore they are depleted in the upper levels, i.e., the ES and the

WL, eventually becoming insufficient for speeding up the QD-SOA gain recovery. Nevertheless, if the current density is concurrently increased, the behavior of the gain is altered in a common manner for all considered changes of τ_{21}, as shown in Fig. 5(b). This means that when investigating the impact of τ_{21} on the switching capability of the AND gate it is also necessary to take into account the simultaneous effect of J.

6. RESULTS FOR AND GATE

In order to examine whether the proposed QD-SOA-based MZI scheme can be configured as ultrafast AND gate at 320 Gb/s we evaluate its performance against the Q-factor. This metric is defined as [73]

$$Q = \frac{\bar{P}_1 - \bar{P}_0}{\sigma_1 + \sigma_0} \tag{6}$$

where $\bar{P}_1$, $\bar{P}_0$ and σ_1, σ_0 are the mean and the standard deviations of the peak power of the marks and spaces, respectively, at the output of the AND gate. In order to ensure acceptable performance, the Q-factor must satisfy the criterion to be over six [73]. Thus in the following we investigate whether this goal can be achieved at 320 Gb/s in terms of the critical operational parameters, which include the peak input data power as well the QD-SOAs small signal gain, current density and electron relaxation time from the ES to the GS.

We begin our simulation analysis by plotting the Q-factor against the peak input data power, P_{peak}, in Fig. 7(a). As it can be observed, the obtained curve exhibits a bell-like variation with a maximum point at around 7.2 dBm, on either side of which the Q-factor is decreased. In order to interpret this behaviour we recall from Fig. 4(a) that the peak input data power determines the extent of the QD-SOA gain excursions, ΔG, which in turn makes the phase difference between the MZI arms lie in different intervals [74]. This affects analogously the magnitude of switching and accordingly the Q-factor. Thus initially the Q-factor is increased with the peak input data power, because QD-SOA1 is progressively brought into deeper saturation and the phase difference approaches closer to its optimum value of π. However as the examined parameter is increased further beyond 7.2 dBm, the additional differential gain that is induced causes the phase difference to diverge away from π [74]. As a result the Q-factor does not continue to improve but it is declined with a steeper slope than that of its rising part due to the stronger carrier depletion. The Q-factor is acceptable within a total input power dynamic range of roughly 4.8 dB, whose central peak power of 7.2 dBm can be provided by commercial erbium doped fiber amplifiers.

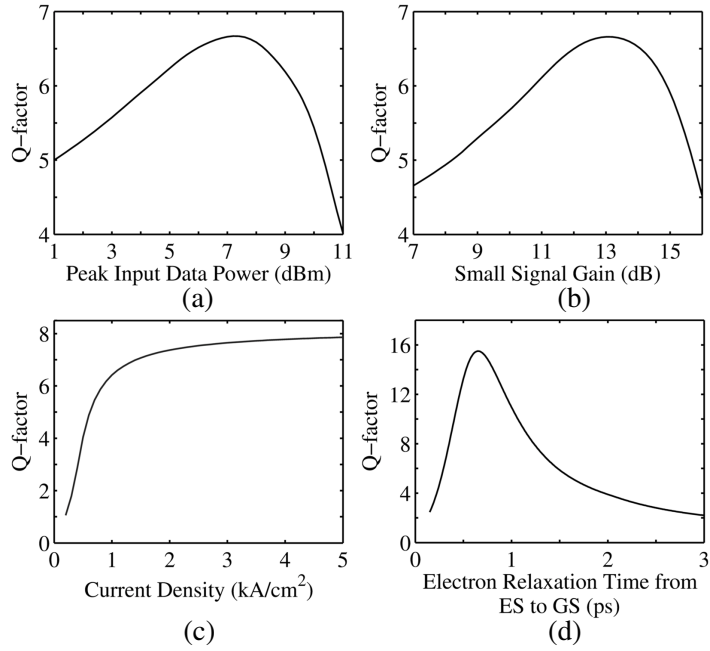

Figure 7. Q-factor variation versus (a) peak input data power, (b) QD-SOAs small signal gain, (c) QD-SOAs current density, (d) QD-SOAs electron relaxation time from the ES to the GS.

Figure 7(b) shows the Q-factor against the QD-SOAs small signal gain. It can be noticed that there is a similarity between the obtained curve and that of Fig. 7(a). This is attributed to the common impact that both parameters have on the QD-SOAs dynamical behaviour, as demonstrated in Section 5. Therefore, as this parameter is altered the phase difference created between the replicas of input data signal B undergoes a variation analogous to that described in the context of Fig. 7(a). This means that in order to achieve switching as anticipated according to the requirements of AND operation an efficient level of small signal gain is necessary. The Q-factor remains above 6 on either side of a small signal gain of approximately 13.2 dB, where it becomes maximum, and within approximately 4 dB. For given QD-SOAs length this small signal gain range can be achieved in a feasible manner by intervening in the number of the QD layers when designing the QD-SOA structure [70]. Here it must be noted that since the small signal gain is determined by the maximum modal gain, which in turn depends on the ratio of the homogeneous to the inhomogeneous broadening [70], this means that the latter are also indirectly accounted

for in the derivation of the results of Fig. 7(b). Given that the homogeneous broadening of QD-SOAs is typically 15 meV at room temperature while the inhomogeneous broadening reaches 40 meV [45], we calculate $g_{\max} = 9.4\,\mathrm{cm}^{-1}$ for $l = 4$ QD layers, which corresponds to $G_{ss} \simeq 13\,\mathrm{dB}$. Now since this value is included in the scanned range of this critical parameter in Fig. 7(b), this means that its impact on the Q-factor is also assessed.

Figure 7(c) illustrates the Q-factor versus the QD-SOAs current density. For small current densities, the Q-factor is sharply increased, and after exceeding its required minimum, it becomes almost independent of this parameter. This happens because a lower current density facilitates the saturation of a QD-SOA [57]. As a result the gain of QD-SOA1 is dropped to a greater extent and it becomes more difficult for it to recover closer to its unsaturated value, which is additionally verified by Fig. 4(c). Consequently, the Q-factor is very low and hence totally inadmissible. In contrast, a larger current density offers a redundancy of supplied carriers and thus permits the dynamical optical properties of QD-SOA1 to reach an equilibrium state, which has a positive impact on the considered metric. Fig. 7(c) shows that if J is adjusted to be over $0.9\,\mathrm{kA/cm}^2$ then the Q-factor is made acceptable. The corresponding bias current is 108 mA, which lies within reasonable limits [57] and can be practically supplied by commercial current sources. Therefore a moderate current density is fine for allowing the proposed AND gate to be realized at least with an adequate performance.

Figure 7(d) depicts the Q-factor as a function of the QD-SOAs electron relaxation time from the ES to the GS. This figure demonstrates that in order for the proposed scheme to operate without logical errors, this parameter must not be chosen arbitrarily fast, as it would be expected from the evidence available on the implementation of another basic logic function using the QD-SOA-based MZI [51]. In fact τ_{21} must not be too small neither too large so as to avoid impairing the quality of switching in terms of the Q-factor. More specifically, for $\tau_{21} > 0.65\,\mathrm{ps}$ the Q-factor starts becoming degraded and as τ_{21} is increased further in this region the performance of the proposed AND gate is strongly deteriorated due to the slower QD-SA1 gain recovery process described in the QD-SOA characterization. On the other hand for $\tau_{21} < 0.65\,\mathrm{ps}$ the very fast relaxation of the carriers from the ES to the GS causes the carrier density in the upper energy levels of the discrete QD-SOA energy diagram to be dramatically decreased. This results in lack of supplied carriers, which limits the ultrafast operation of the MZI and renders the Q-factor unacceptable. Thus we need to take jointly into account the contribution of the current density,

as inferred from the discussion of the QD-SOA characterization. To this end the current density must be properly chosen as specified from Fig. 7(c). The Q-factor remains over 6 against τ_{21} within approximately 1.17 ps. The values lying in this range as well as the maximum of 0.65 ps are typical for τ_{21} [45].

From the observation and interpretation of Figs. 7(a)–(d) it can be deduced that the requirements for the critical parameters are $4.4\,\text{dBm} \leq P_{\text{peak}} \leq 9.2\,\text{dBm}$, $10.8\,\text{dB} \leq G_{ss} \leq 14.8\,\text{dB}$, $J \geq 0.9\,\text{kA/cm}^2$ and $0.3\,\text{ps} \leq \tau_{21} \leq 1.47\,\text{ps}$. Thus by following these guidelines and using the combination of values 9 dBm, 14 dB, $1.5\,\text{kA/cm}^2$ and 0.6 ps, respectively, a more than adequate Q-factor can be achieved. This is reflected on the results obtained for the representative data patterns A = '1011011110110001' (Fig. 8(a)) and B = '1001010101111111' (Fig. 8(b)). Indeed the logical outcome in Fig. 8(c) coincides with the truth table of the Boolean AND function since a mark is produced only when the binary content of A and B is identical while a space occurs in all other cases. Furthermore the zeros are strongly suppressed, which corresponds to ER = 13.3 dB. Concurrently the marks are sufficiently balanced and the difference between their peak amplitudes is only 0.1 dB, as verified by Fig. 9 and the uniform drop of QD-SOA1 gain in response to data signal A. The good quality of the AND operation is also confirmed by the corresponding pseudo-eye diagram (PED) [75] which has been plotted

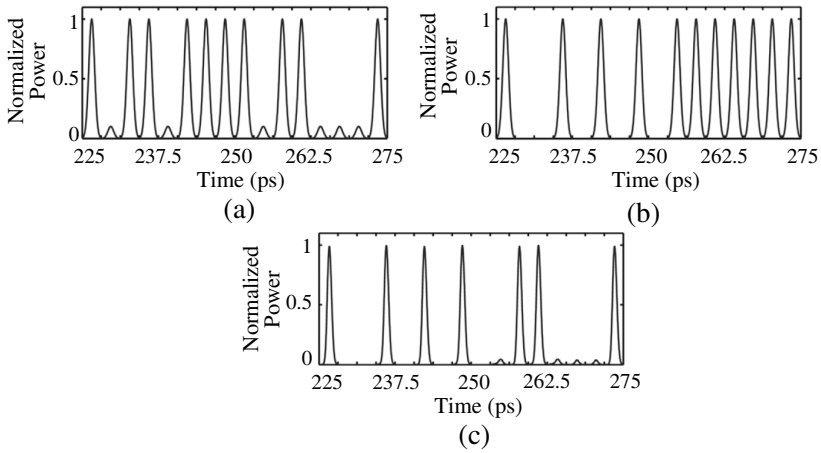

Figure 8. Simulation results for the specified suitable choice of critical parameters: (a) data stream A, (b) data stream B, (c) logical outcome of A AND B operation.

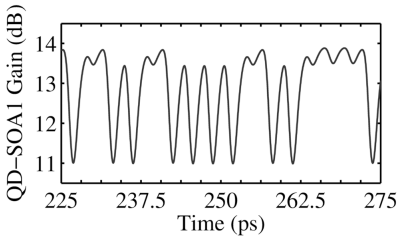

Figure 9. Gain response of QD-SOA1 to data stream A of Fig. 8(a).

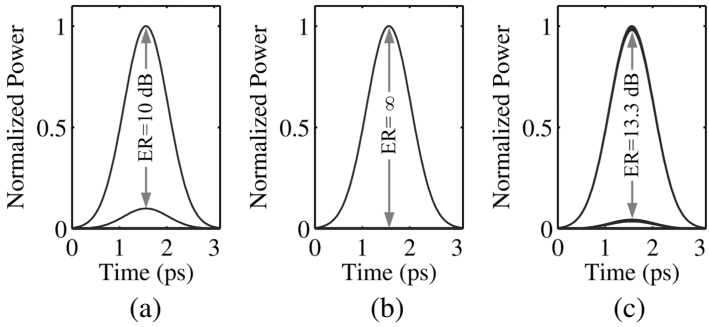

Figure 10. Simulated pseudo-eye diagrams of (a) data A, (b) data B, (c) A AND B operation with corresponding extinction ratios (ER) indicated.

in Fig. 10(c) for a 127 bit-long data stream. This visual quality indicator is obtained by superimposing the marks and spaces in the data stream of interest on top of each other and displaying them within a single bit period. According to this generation method the PED consists in the general case of two distinct curves, one for the marks and one for the spaces, while its form depends on the quality of these bits, both individually and in relation to each other. For example, for data A the marks are equal in intensity, which is directly reflected on the curve having the highest amplitude. However, as mentioned in Subsection 4.2, in order to conduct a simulation analysis as realistic as possible, all spaces of this signal are not fully extinguished, as it would happen in the ideal case, but they have a finite extinction ratio of 10 dB. Consequently, these bits also exhibit a single curve, but its vertical distance from that of the marks is analogous to their ER indicated inside the PED. In comparison in the PED of signal B depicted in Fig. 10(b) there is no curve shown for the spaces because the ER is perfect and consequently the power of these bits is null. Thus based on this qualitative explanation, we can similarly interpret the PED of the logical outcome A AND B in Fig. 10(c). Therefore, the spaces

have acquired a single and suppressed border, and the envelope of the marks is uniform since their traces almost coincide, having a hardly discernible difference between their peaks. This indicates that the PED is clear and open, and that owing to its proper design, the proposed AND gate can be realized with error-free performance.

7. CONCLUSION

In conclusion, the feasibility of realizing an all-optical AND gate between a pair of fully-loaded data sequences at 320 Gb/s using a properly driven QD-SOA-MZI has been theoretically investigated and demonstrated. By conducting numerical simulation, a set of curves has been obtained for the impact of the involved critical parameters on the Q-factor. Based on a detailed characterization of the dynamical behavior of a QD-SOA that is subject to an ultrafast data pulse stream, the simulation results have been analyzed and interpreted. In this manner, the operating conditions, which are favorable in order for the employed metric to meet its desired criterion, have been derived. These suggest that it would be possible to achieve the pursued logic function with error-free performance and high quality for a combination of moderate values for all involved parameters, which can be well supported by state-of-the-art QD-SOA technology. This prediction can enhance the capability of the QD-SOA-based MZI as switching module, complement the suite of bitwise Boolean functions that it can execute and facilitate its exploitation in more sophisticated circuits and subsystems.

REFERENCES

1. Houbavlis, T., K. E. Zoiros, M. Kalyvas, G. Theophilopoulos, C. Bintjas, K. Yiannopoulos, N. Pleros, K. Vlachos, H. Avramopoulos, L. Schares, L. Occhi, G. Guekos, J. R. Taylor, S. Hansmann, and W. Miller, "All-optical signal processing and applications within the Esprit project DO_ALL," *Journal of Lightwave Technology*, Vol. 23, No. 2, 781–801, 2005.
2. Zoiros, K. E., T. Houbavlis, and M. Kalyvas, "Ultra-high speed all-optical shift registers and their applications in OTDM networks," *Optical and Quantum Electronics*, Vol. 36, No. 11, 1005–1053, 2004.
3. Hamilton, S. A., B. S. Robinson, T. E. Murphy, S. J. Savage, and E. P. Ippen, "100 Gb/s optical time-division multiplexed networks," *Journal of Lightwave Technology*, Vol. 20, No. 12, 2086–2100, 2002.

4. De Melo, A. M., S. Randel, and K. Petermann, "Mach-Zehnder interferometer-based high-speed OTDM add-drop multiplexing," *Journal of Lightwave Technology*, Vol. 25, No. 4, 1017–1026, 2007.
5. Kanellos, G. T., L. Stampoulidis, N. Pleros, T. Houbavlis, D. Tsiokos, E. Kehayas, H. Avramopoulos, and G. Guekos, "Clock and data recovery circuit for 10-Gb/s asynchronous optical packets," *IEEE Photonics Technology Letters*, Vol. 15, No. 11, 1666–1668, 2003.
6. Ji, W., M. Zhang, and P. Ye, "All-optical-packet header and payload separation for unslotted optical-packet-switched networks," *Journal of Lightwave Technology*, Vol. 25, No. 3, 703-709, 2007.
7. Webb, R. P., X. Yang, R. J. Manning, G. D. Maxwell, A. J. Poustie, S. Lardenois, and D. Cotter, "All-optical binary pattern recognition at 42 Gb/s," *Journal of Lightwave Technology*, Vol. 27, No. 13, 2240–2245, 2009.
8. Wang, J., G. Meloni, G. Berrettini, L. Potì, and A. Bogoni, "All-optical clocked flip-flops and binary counting operation using SOA-based SR latch and logic gates," *IEEE Journal of Selected Topics in Quantum Electronics*, Vol. 16, No. 5, 1486–1494, 2010.
9. Ghaffari, B. M. and J. A. Salehi, "Applications and performance of optical analog-to-digital converter and optical logic gate elements in multilevel multiclass fiber-optic CDMA systems," *IEEE Journal of Selected Topics in Quantum Electronics*, Vol. 16, No. 5, 1476–1485, 2010.
10. Wang, Y., X. Zhang, J. Dong, and D. Huang, "Simultaneous demonstration on all-optical digital encoder and comparator at 40 Gb/s with semiconductor optical amplifiers," *Optics Express*, Vol. 15, No. 23, 15080–15085, 2007.
11. Leclerc, O., B. Lavigne, E. Balmefrezol, P. Brindel, L. Pierre, D. Rouvillain, and F. Seguineau, "Optical regeneration at 40 Gb/s and beyond," *Journal of Lightwave Technology*, Vol. 21, No. 11, 2779–2790, 2003.
12. Westlund, M., P. A. Andrekson, H. Sunnerud, J. Hansryd, and J. Li, "High performance optical-fiber-nonlinearity-based optical waveform monitoring," *Journal of Lightwave Technology*, Vol. 23, No. 6, 2012–2022, 2005.
13. Kim, S. H., J. H. Kim, J. W. Choi, C. W. Son, Y. T. Byun, Y. M. Jhon, S. Lee, D. H. Woo, and S. H. Kim, "All-optical half adder using cross gain modulation in semiconductor optical amplifiers," *Optics Express*, Vol. 14, No. 22, 10693–10698, 2006.
14. Gayen, D. K., T. Chattopadhyay, R. K. Pal, and J. N. Roy,

"All-optical multiplication with the help of semiconductor optical amplifier-assisted Sagnac switch," *Journal of Computational Electronics*, Vol. 9, No. 2, 57–67, 2010.

15. Kumar, S. and A. E. Willner, "Simultaneous four-wave mixing and cross-gain modulation for implementing an all-optical XNOR logic gate using a single SOA," *Optics Express*, Vol. 14, No. 12, 5092–5097, 2006.
16. Jung, Y. J., C. W. Son, Y. M. Jhon, S. Lee, and N. Park, "One-level simplification method for all-optical combinational logic circuits," *IEEE Photonics Technology Letters*, Vol. 20, No. 10, 800–802, 2008.
17. Dagens, B., A. Labrousse, R. Brenot, B. Lavigne, and M. Renaud, "SOA-based devices for all-optical signal processing," *Proceedings of Optical Fiber Communication Conference*, ThX1, 582–583, 2003.
18. Ying, C.-L., H.-H. Lu, W.-S. Tsai, H.-C. Peng, and C.-H. Lee, "To employ SOA-based optical SSB modulation technique in full-duplex RoF transport system," *Progress In Electromagnetics Research Letters*, Vol. 7, 1–13, 2009.
19. Wu, J.-W., D.-X. Tian, and H.-B. Bao, "A designed model about amplification and compression of picoseconds pulse using cascaded SOA and NOLM device," *Progress In Electromagnetics Research*, Vol. 76, 127–139, 2007.
20. Ying, C.-L., C.-H. Chang, Y.-L. Houng, H.-H. Lu, W.-S. Tsai, and H.-S. Su, "Down link CATV/FTTH and up-link FFTH transport systems based on reflective semiconductor opticalamplifier," *Progress In Electromagnetics Research C*, Vol. 11, 109–120, 2009.
21. Soto, H., C. A. Díaz, J. Topomondzo, D. Erasme, L. Schares, and G. Guekos, "All-optical AND gate implementation using cross-polarization modulation in a semiconductor optical amplifier," *IEEE Photonics Technology Letters*, Vol. 14, No. 4, 498–500, 2002.
22. Kim, J. H., B. C. Kim, Y. T. Byun, Y. M. Jhon, S. Lee, D. H. Woo, and S. H. Kim, "All-optical AND gate using cross-gain modulation in semiconductor optical amplifiers," *Japanese Journal of Applied Physics*, Vol. 43, No. 2, 608–610, 2004.
23. Zhang, X., Y. Wang, J. Sun, D. Liu, and D. Huang, "All-optical AND gate at 10 Gbit/s based on cascaded single-port-coupled SOAs," *Optics Express*, Vol. 12, No. 3, 361–366, 2004.
24. Sharaiha, A., J. Topomondzo, and P. Morel, "All-optical logic AND-NOR gate with three inputs based on cross-gain modulation in a semiconductor optical amplifier," *Optics Communications*, Vol. 265, No. 1, 322–325, 2006.

25. Berrettini, G., A. Simi, A. Malacarne, A. Bogoni, and L. Potì, "Ultrafast integrable and reconfigurable XNOR, AND, NOR, and NOT photonic logic gate," *IEEE Photonics Technology Letters*, Vol. 18, No. 8, 917–919, 2006.
26. Li, Z. and G. Li, "Ultrahigh-speed reconfigurable logic gates based on four-wave mixing in a semiconductor optical amplifier," *IEEE Photonics Technology Letters*, Vol. 18, No. 12, 1341–1343, 2006.
27. Guo, L. Q. and M. J. Connelly, "All-optical AND gate with improved extinction ratio using signal induced nonlinearities in a bulk semiconductor optical amplifier," *Optics Express*, Vol. 14, No. 7, 2938–2943, 2006.
28. Patel, N. S., K. L. Hall, and K. A. Rauschenbach, "Interferometric all-optical switches for ultrafast signal processing," *Applied Optics*, Vol. 37, No. 14, 2831–2841, 1998.
29. Dong, H., H. Sun, Q. Wang, N. K. Dutta, and J. Jaques, "80 Gb/s all-optical logic AND operation using Mach-Zehnder interferometer with differential scheme," *Optics Communications*, Vol. 265, No. 1, 79–83, 2006.
30. Feng, C., J. Wu, K. Xu, and J. Lin, "Simple ultrafast all-optical AND logic gate," *Optical Engineering*, Vol. 46, No. 12, Art. No. 125006, 2007.
31. Martínez, J. M., F. Ramos, and J. Martí, "10 Gb/s reconfigurable optical logic gate using a single hybrid-integrated SOA-MZI," *Fiber and Integrated Optics*, Vol. 27, No. 1, 15–23, 2008.
32. Singh, S. and Lovkesh, "Ultrahigh speed optical signal processing logic based on an SOA-MZI," *IEEE Journal of Selected Topics in Quantum Electronics*, Vol. 18, No. 2, 970–977, 2012.
33. Mørk, J., M. L. Nielsen, and T. W. Berg, "The dynamics of semiconductor optical amplifiers: Modeling and applications," *Optics and Photonics News*, Vol. 14, No. 7, 42–48, 2003.
34. Mulvad, H. C. H., M. Galili, L. K. Oxenløwe, H. Hu, A. T. Clausen, J. B. Jensen, C. Peucheret, and P. Jeppesen, "Demonstration of 5.1 Tb/s data capacity on a single-wavelength channel," *Optics Express*, Vol. 18, No. 2, 1438–1443, 2010.
35. Ji, W., M. Zhang, and P. Ye, "Simulation of an all-optical XOR gate with a semiconductor optical amplifier Mach-Zehnder interferometer sped up by a continuous-wave assistant light," *Journal of Optical Networking*, Vol. 4, No. 8, 524–530, 2005.
36. Randel, S., A. M. de Melo, K. Petermann, V. Marembert, and C. Schubert, "Novel scheme for ultrafast all-optical XOR operation," *Journal of Lightwave Technology*, Vol. 22, No. 12,

2808–2815, 2004.

37. Sun, H., Q. Wang, H. Dong, Z. Chen, N. K. Dutta. J. Jaques, and A. B. Piccirilli, "All-optical logic XOR gate at 80 Gb/s using SOA-MZI-DI," *IEEE Journal of Quantum Electronics*, Vol. 42, No. 8, 747–751, 2006.
38. Gutiérrez-Castrejón, R., "Turbo-switched Mach-Zehnder interferometer performance as all-optical signal processing element at 160 Gb/s," *Optics Communications*, Vol. 282, No. 22, 4345–4352, 2009.
39. Webb, R. P., R. J. Manning, G. D. Maxwell, and A. J. Poustie, "40 Gbit/s all-optical XOR gate based on hybrid-integrated Mach-Zehnder interferometer," *Electronics Letters*, Vol. 39, No. 1, 79–81, 2003.
40. Kang, I., M. Rasras, L. Buhl, M. Dinu, S. Cabot, M. Cappuzzo, L. T. Gomez, Y. F. Chen, S. S. Patel, N. Dutta, A. Piccirilli, J. Jaques, and C. R. Giles, "All-optical XOR and XNOR operations at 86.4 Gb/s using a pair of semiconductor optical amplifier Mach-Zehnder interferometers," *Optics Express*, Vol. 17, No. 21, 19062–19066, 2009.
41. Berg, T. W. and J. Mørk, "Saturation and noise properties of quantum-dot optical amplifiers," *IEEE Journal of Quantum Electronics*, Vol. 40, No. 11, 1527–1539, 2004.
42. Akiyama, T., M. Ekawa, M. Sugawara, K. Kawaguchi, H. Sudo, A. Kuramata, H. Ebe, and Y. Arakawa, "An ultrawide-band semiconductor optical amplifier having an extremely high penalty-free output power of 23 dBm achieved with quantum dots," *IEEE Photonics Technology Letters*, Vol. 17, No. 8, 1614–1616, 2005.
43. Yasuoka, N., K. Kawaguchi, H. Ebe, T. Akiyama, M. Ekawa, K. Morito, M. Sugawara, and Y. Arakawa, "Quantum-dot semiconductor optical amplifiers with polarization-independent gains in 1.5-μm wavelength bands," *IEEE Photonics Technology Letters*, Vol. 20, No. 23, 1908–1910, 2008.
44. Zilkie, A. J., J. Meier, M. Mojahedi, P. J. Poole, P. Barrios, D. Poitras, T. J. Rotter, C. Yang, A. Stintz, K. J. Malloy, P. W. E. Smith, and J. Stewart Aitchison, "Carrier dynamics of quantum-dot, quantum-dash and quantum-well semiconductor optical amplifiers operating at 1.55 μm," *IEEE Journal of Quantum Electronics*, Vol. 43, No. 11, 982–991, 2007.
45. Sugawara, M., T. Akiyama, N. Hatori, Y. Nakata, H. Ebe, and H. Ishikawa, "Quantum-dot semiconductor optical amplifiers for high-bit-rate signal processing up to 160 Gbs-1 and a new scheme of 3R regenerators," *Measurement Science and Technology*,

Vol. 13, No. 11, 1683–1691, 2002.

46. Uskov, A. V., E. P. O'Reilly, R. J. Manning, R. P. Webb, D. Cotter, M. Laemmlin, N. N. Ledentsov, and D. Bimberg, "On ultrafast optical switching based on quantum-dot semiconductor optical amplifiers in nonlinear interferometers," *IEEE Photonics Technology Letters*, Vol. 16, No. 5, 1265–1267, 2004.
47. Schreieck, R. P., M. H. Kwakernaak, H. Jäckel, and H. Melchior, "All-optical switching at multi-100-Gb/s data rates with Mach-Zehnder interferometer switches," *IEEE Journal of Quantum Electronics*, Vol. 38, No. 8, 1053–1061, 2002.
48. Sun, H., Q. Wang, H. Dong, and N. K. Dutta, "All-optical logic performance of quantum-dot semiconductor amplifier-based devices," *Microwave and Optical Technology Letters*, Vol. 48, No. 1, 29–35, 2006.
49. Han, H., M. Zhang, P. Ye, and F. Zhang, "Parameter design and performance analysis of an ultrafast all-optical XOR gate based on quantum dot semiconductor optical amplifiers in nonlinear Mach-Zehnder interferometer," *Optics Communications*, Vol. 281, No. 20, 5140–5145, 2008.
50. Ben-Ezra, Y., B. I. Lembrikov, and M. Haridim, "Ultrafast all-optical processor based on quantum-dot semiconductor optical amplifiers," *IEEE Journal of Quantum Electronics*, Vol. 45, No. 1, 34–41, 2009.
51. Rostami, A., H. B. A. Nejad, R. M. Qartavol, and H. R. Saghai, "Tb/s optical logic gates based on quantum-dot semiconductor optical amplifiers," *IEEE Journal of Quantum Electronics*, Vol. 46, No. 3, 354–360, 2010.
52. Dimitriadou, E. and K. E. Zoiros, "On the design of ultrafast all-optical NOT gate using quantum-dot semiconductor optical amplifier-based Mach-Zehnder interferometer," *Optics and Laser Technology*, Vol. 44, No. 3, 600–607, 2012.
53. Dimitriadou, E. and K. E. Zoiros, "Proposal for all-optical NOR gate using single quantum-dot semiconductor optical amplifier-based Mach-Zehnder interferometer," *Optics Communications*, Vol. 285, No. 7, 1710–1716, 2012.
54. Dimitriadou, E. and K. E. Zoiros, "On the feasibility of ultrafast all-optical NAND gate using single quantum-dot semiconductor optical amplifier-based Mach-Zehnder interferometer," *Optics and Laser Technology*, Vol. 44, No. 6, 1971–1981, 2012.
55. Dimitriadou, E. and K. E. Zoiros, "On the design of reconfigurable ultrafast all-optical NOR and NAND gates using a single quantum-dot semiconductor optical amplifier-based Mach-

Zehnder interferometer," *Journal of Optics*, Vol. 14, No. 10, Art. No. 105401, 2012.

56. Dimitriadou, E. and K. E. Zoiros, "Proposal for ultrafast all-optical XNOR gate using single quantum-dot semiconductor optical amplifier-based Mach-Zehnder interferometer," *Optics and Laser Technology*, Vol. 45, No. 1, 79–88, 2013.
57. Yang, W., M. Zhang, and P. Ye, "Analysis of all-optical demultiplexing from 160/320 Gbit/s to 40 Gbit/s using quantum-dot semiconductor optical amplifiers assisted Mach-Zehnder interferometer," *Microwave and Optical Technology Letters*, Vol. 52, No. 7, 1629–1633, 2010.
58. Papadopoulos, G. and K. E. Zoiros, "On the design of semiconductor optical amplifier-assisted Sagnac interferometer with full data dual output switching capability," *Optics and Laser Technology*, Vol. 43, No. 3, 697–710, 2011.
59. Qasaimeh, O., "An analytical model for quantum dot semiconductor optical amplifiers," *Optics Communications*, Vol. 222, No. 1–6, 277–287, 2003.
60. Barnham, K. and D. D. Vvdensky, *Low-dimensional Semiconductor Structures: Fundamentals and Device Applications*, Cambridge University Press, 2001.
61. Scheel, H. J. and P. Capper, *Crystal Growth Technology: From Fundamentals and Simulation to Large-scale Production*, Wiley-VCH, Weinheim, 2008.
62. Ben-Ezra, Y., B. I. Lembrikov, and M. Haridim, "Acceleration of gain recovery and dynamics of electrons in QD-SOA," *IEEE Journal of Quantum Electronics*, Vol. 41, No. 10, 1268–1273, 2005.
63. Ben-Ezra, Y., B. I. Lembrikov, and M. Haridim, "Specific features of XGM in QD-SOA," *IEEE Journal of Quantum Electronics*, Vol. 43, No. 8, 730–737, 2007.
64. Ben-Ezra, Y., M. Haridim, B. I. Lembrikov, and M. Ran, "Proposal for all-optical generation of ultra-wideband impulse radio signals in Mach-Zehnder interferometer with quantum-dot optical amplifier," *IEEE Photonics Technology Letters*, Vol. 20, No. 7, 484–486, 2008.
65. Majer, N., K. Lüdge, and E. Schöll, "Cascading enables ultrafast gain recovery dynamics of quantum dot semiconductor optical amplifiers," *Physical Review B*, Vol. 82, Art. No. 235301, 2010.
66. Hamié, A., M. Hamze, J. L. Wei, A. Sharaiha, and J. M. Tang, "Theoretical investigations of quantum-dot semiconductor optical amplifier enabled intensity modulation of adaptively modulated

optical OFDM signals in IMDD PON systems," *Optics Express*, Vol. 19, No. 25, 25696–25711, 2011.

67. Li, X. and G. Li, "Comments on 'theoretical analysis of gain recovery time and chirp in QD-SOA'," *IEEE Photonics Technology Letters*, Vol. 18, No. 22, 2434–2435, 2006.
68. Sygletos, S., M. Spyropoulou, P. Vorreau, R. Bonk, I. Tomkos, W. Freude, and J. Leuthold, "Multi-wavelength regenerative amplification based on quantum-dot semiconductor optical amplifiers," *Proceedings of International Conference on Transparent Optical Networks*, We.D2.5, 234–237, 2007.
69. Bogoni, A., L. Potì, P. Ghelfi, M. Scaffardi, C. Porzi, F. Ponzini, G. Meloni, G. Berrettini, A. Malacarne, and G. Prati, "OTDM-based optical communications networks at 160 Gbit/s and beyond," *Optical Fiber Technology*, Vol. 13, No. 1, 1–12, 2007.
70. Uskov, A. V., J. Mørk, B. Tromborg, T. W. Berg, I. Magnusdottir, and E. P. O'Reilly, "On high-speed cross-gain modulation without pattern effects in quantum dot semiconductor optical amplifiers," *Optics Communications*, Vol. 227, No. 4–6, 363–369, 2003.
71. Zilkie, A. J., J. Meier, M. Mojahedi, A. S. Helmy, P. J. Poole, P. Barrios, D. Poitras, T. J. Rotter, C. Yang, A. Stintz, K. J. Malloy, P. W. E. Smith, and J. S. Aitchison, "Time-resolved linewidth enhancement factors in quantum dot and higher-dimensional semiconductor amplifiers operating at 1.55 μm," *Journal of Lightwave Technology*, Vol. 26, No. 11, 1498–1509, 2008.
72. Yang, W., M. Zhang, and P. Ye, "Analysis of 160 Gb/s all-optical NRZ-to-RZ data format conversion using quantum-dot semiconductor optical amplifiers assisted Mach-Zehnder interferometer," *Optics Communications*, Vol. 282, No. 9, 1744–1750, 2009.
73. Agrawal, G. P., *Fiber-optic Communication Systems*, Wiley, New York, 2002.
74. Zoiros, K. E., P. Avramidis, and C. S. Koukourlis, "Performance investigation of semiconductor optical amplifier-based ultrafast nonlinear interferometer in nontrivial switching mode," *Optical Engineering*, Vol. 47, No. 11, Art. No. 115006, 2008.
75. Gutiérrez-Castrejón, R., L. Occhi, L. Schares, and G. Guekos, "Recovery dynamics of cross-modulated beam phase in semiconductor amplifiers and applications to all-optical signal processing," *Optics Communications*, Vol. 195, No. 1–4, 167–1771, 2001.